28th European Young Geotechnical Engineers Conference – EYGEC 2024
 ISBN xxx-xxx-xx-xxxx-x

Clay experimental study and cracking mechanisms under controlled desiccation paths using digital image correlation

Lamine Ighil Ameur[a], and Mahdia Hattab[b]

[a] *Cerema, GéoCoD: Géomatériaux et Géomécanique: couplages et dynamique pour les risques et les ouvrages géotechniques, Blois, France*
[b] *Laboratoire d'études des microstructures et de mécanique des matériaux (UMR7239), Université de Lorraine, Metz, France*

ABSTRACT

The aim of this research is to characterize the shrinkage phenomenon and the cracking mechanisms of a clayey soil subjected to the controlled desiccation in a laboratory experimental system. The approach consisted first to carry out a series of different controlled desiccation tests under three suction levels: high in 361MPa, middle in 110MPa and low in 38MPa. Using the digital image correlation (DIC) method, total local strains were measured. Drying and shrinkage kinetics analysis showed that strains are probably due to both a shrinkage part and another part that can be named "mechanical". Only the mode I of cracking mechanisms was observed basing only on calculations of the principal "mechanical" strains.

KEYWORDS

Clay; Desiccation; Cracking; Image Correlation; Shrinkage, Critical strains.

1. INTRODUCTION

The presence of cracks in a soil mass induces the creation of some zones of weak tension that drop down the mechanical resistance (Morris et al., 1992). Thus, this can have a significant impact on the hydraulic conductivity of clayey soils, which increases with the development of cracks. Relative humidity and temperature are the mainly influencing parameters during controlled desiccation tests. This can be characterized by a direct modification on drying variables such as: water content, saturation degree, shrinkage limit and local suction of the soil.

Desiccation cracking of clayey soils usually occurred when the developed tensile stress due to suction exceeds the tensile strength of the soil (Kodikara et al., 1999). Tensile stresses develop only in the case where the soil is restricted against shrinkage. This restriction can be external due to the interface of a rough layer for example or internal due to some parts of soil during non-uniform drying for example.

This research is mainly focused on the characterization of shrinkage phenomenon and understanding how controlled desiccation cracking initiate and propagate through a clayey material. A series of controlled desiccation tests where then performed under three levels of imposed suction. The experimental approach aims to estimate shrinkage using the digital image correlation (DIC) method and allows calculating a critical value of the mechanical local strain acting the cracking.

2. MATERIAL AND METHOD

2.1. Material properties and sample preparation

The tested clayey material employed in this study was *Kaolinite K13*, which is an industrial clay marketed by *Sibelco* (Paris, France). Some of its physical properties are: liquid limit, $w_L = 40\%$; plastic limit, $w_P = 20\%$; density of the solid grains, $\gamma_s/\gamma_w = 2.65$; and shrinkage limit, $w_{SL} = 16\%$. This synthetic clay appears to be similar to the well-known *Kaolinite P300*. An elementary Kaolinite particle consists of a set of stacked sheets as described in Hattab et al. (2014). The mineralogical analysis of Kaolinite P300, carried out using X-ray diffraction technique performed by Hammad et al. (2013), reveals that in addition to Kaolinite, various secondary minerals such as Illite and Quartz have also been identified.

Soil samples were made by spreading mixed slurry with an initial water content $w_0 = 1.2\ w_L$ on a rectangular Teflon support. The dimensions of each specimen are 190 mm in length, 130 mm in width and 4 mm in thickness. The upper surface of soil sample was flecked with small and very dense spots of dark paint spraying. This was necessary for DIC calculations needing different grey levels.

2.2. Test equipment

The experimental device developed for this study is shown in Fig. 1 as a control chamber of glass used to create a confined volume for applying the Vapor Equilibrium Technique (VET) described in *section 2.4*. It is able to combine two techniques for performing controlled desiccation tests: (i) a balance with 0.1g accuracy to follow water content evolution, salt solution to impose the hygrometric parameters (relative humidity and temperature) that were measured with a hygrometer; (ii) DIC method which needs an HD camera to take images every fixed time interval, a computer to save the images and allows running calculations with Vic2D software which leads an accuracy about 3% for displacements.

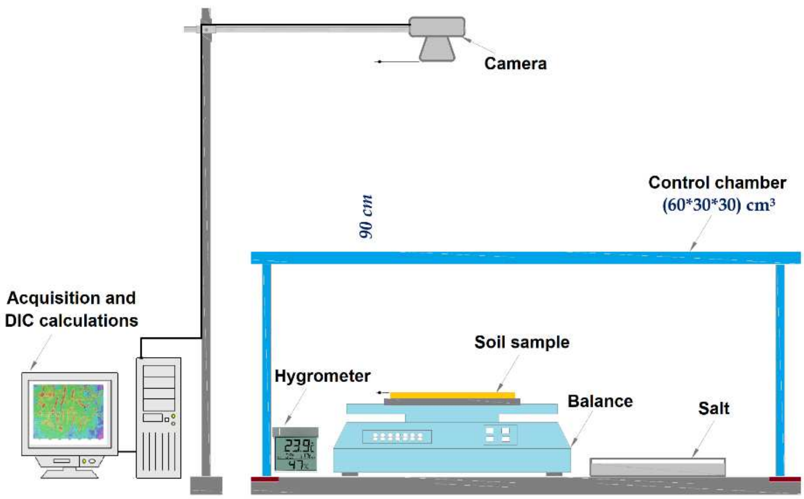

Figure 1. Experimental controlled desiccation test apparatus

To carry out the two-dimensional DIC method, Vic2D software was used similarly to that of Wei et al. (2016). It provides the displacement and strain fields to analyse precisely the local behaviour of the material during controlled desiccation paths.

2.3. DIC method parameters and Vic2D software

Before using Vic2D software, some parameters should be defined (Fig. 2): (i) scale calibration to convert pixels of saved images to milimiters of displacements, 1 pixel = 0.11 mm; (ii) subset = 17 and step = 5 of the selected area into the image, important parameters that allow to optimize DIC calculations in terms of the correlation quality and time needed to finish the run.

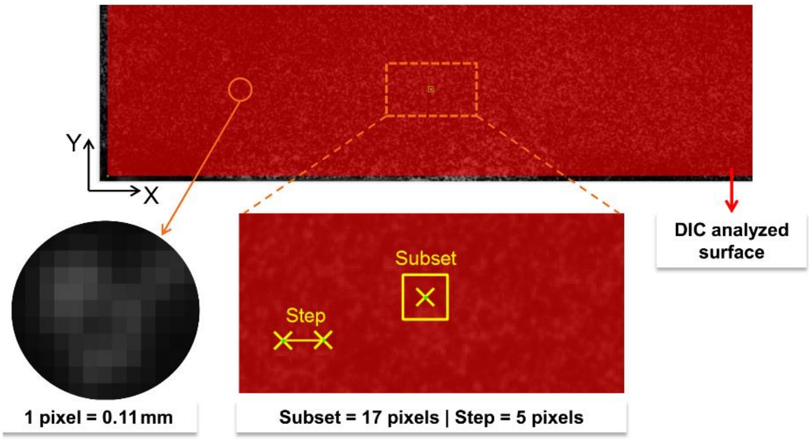

Figure 2. DIC parameters on Vic2D software

The outputs of running Vic2D software are: (i) displacements, u (mm) along the X-axis, and v (mm) along the Y-axis; (ii) strains generated in post-processing, ε_{xx} (%) normal component of strain in the X-direction, ε_{yy} (%) normal component of strain in the Y-direction, and ε_{xy} (%) shear strain.

2.4. Salt solutions technique characteristics

Controlled desiccation tests were performed using salt solutions technique based on Kelvin's law. Thus, the Equation (1), given by Fredlund and Rahardjo (1993), allows determining the imposed global suction s_{glob} (MPa) as a function of relative humidity *RH* and thermodynamic temperature *T* inside the control chamber.

$$s_{glob} = -\frac{\rho_w RT}{M_w} ln\left(\frac{RH\%}{100}\right) \quad (1)$$

where M_w *is the molar mass of water*, *R is the molar gas constant and* ρ_w *is volumetric mass of water*.

Three suction levels were fixed in this study corresponding to three salt solutions, selected according to the conditions cited in Delage et al. (1998):

(i) high in 361±11MPa using KOH;
(ii) middle in 110±5.7MPa using K_2CO_3;
(iii) low in 38±9.8MPa using NaCl.

Test names are given following this nomenclature: CD (controlled desiccation) _Test number (1 to 3) _Mean value of s_{glob} (MPa). Example: CD2-s361 (test number 2 for high suction level).

3. RESULTS AND DISCUSSION

3.1. Drying evolution under controlled desiccation path

Figure 3 shows the drying curves evolution under each suction level. The results highlight that drying velocity, defined by *dw/dt* (%/h), changes with suction level. Three characteristic intervals of time can be identified for each curve:

(i) first stage from t_1 to t_2, where the mean value of drying velocity noted $(dw/dt)_m$ is calculated;
(ii) second stage where t_2 is the beginning of drying velocity decrease and tends to zero at t_3;
(iii) final stage for $t > t_3$, *dw/dt* equals zero meaning there is no drying more.

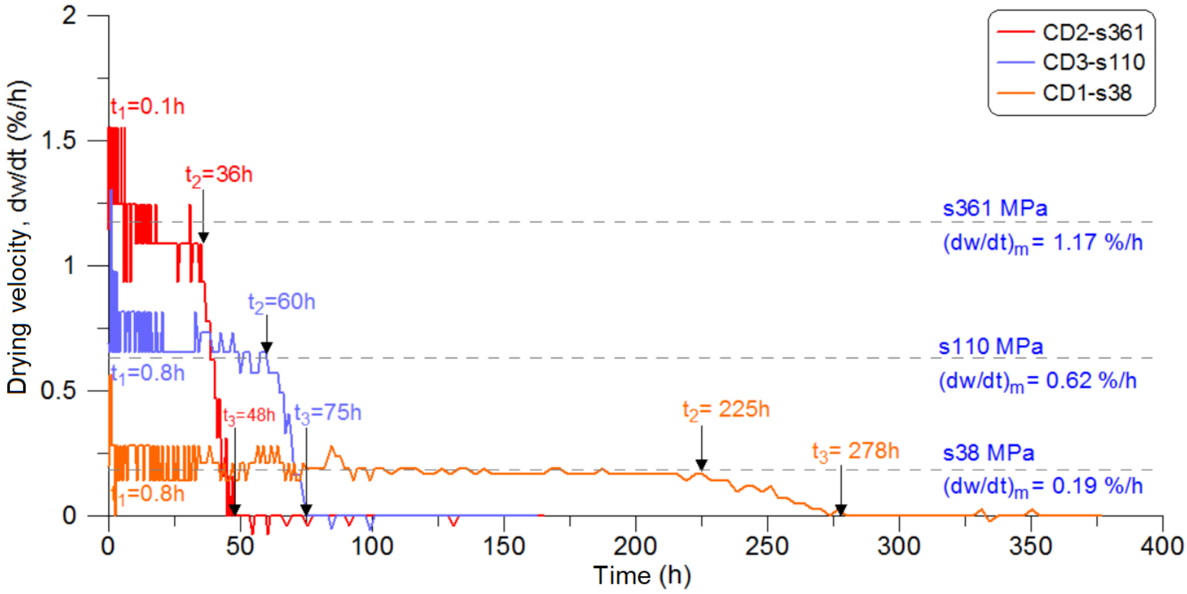

Figure 3. Drying velocity under different suction levels during controlled desiccation path (m = mean value)

3.2. Shrinkage phenomenon: analysis at the global scale

In order to analyse the shrinkage kinetic during drying, a shrinkage velocity was determined from an estimated volumetric strain defined by $d\varepsilon_v/dt$ (%/h) and plotted as a function of time on Figure 4. The results show a similar trend of curves compared to that of drying velocity (Figure 3) with an evolution in three stages. Here, time t_3 represents the shrinkage limit time t_{SL}. This comparison highlights that t_2 and t_{SL} on Figure 4 are less than t_2 and t_3 on Figure 3, respectively at each suction level. When shrinkage stops, drying of soil sample continues to happen and tends to zero later more.

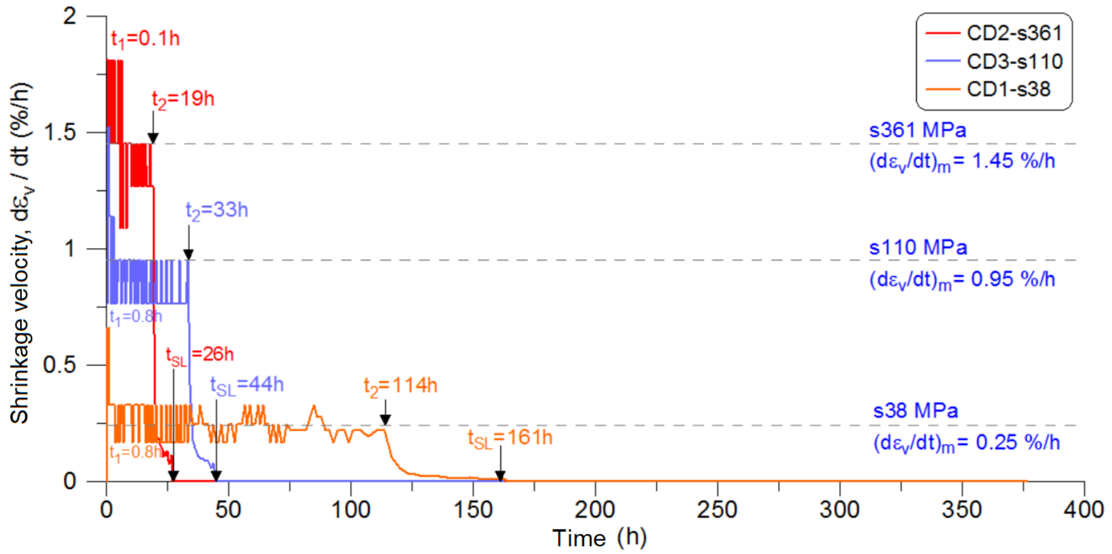

Figure 4. Shrinkage velocity under different suction levels during controlled desiccation path (m = mean value)

3.3. Discussion: controlled desiccation cracking

Only mode I (opening mode), developed in Ighil Ameur and Hattab (2022) through bending tests, was observed in all cracks of this study developed under high suction level. Generally, cracks initiate from edges and propagate to the center of soil sample. Two edge-cracking zones are localized on ε_{xx} and ε_{yy} maps shown in Figure 5 (a) and (b) and named *III-CD2-s361* and *II-CD2-s361*, respectively. To highlight this cracking mechanism (mode I), principal “mechanical” strains analysis were carried out using a calculation program developed by Wei (2014). The results are shown in Figure 5 (a’) and (b’) for *III-CD2-s361* and *II-CD2-s361*, respectively. In these two zones, extension characterized by many long red vectors appears very dense and all perpendicular to the direction of the crack. This confirms the crack initiation by mode I.

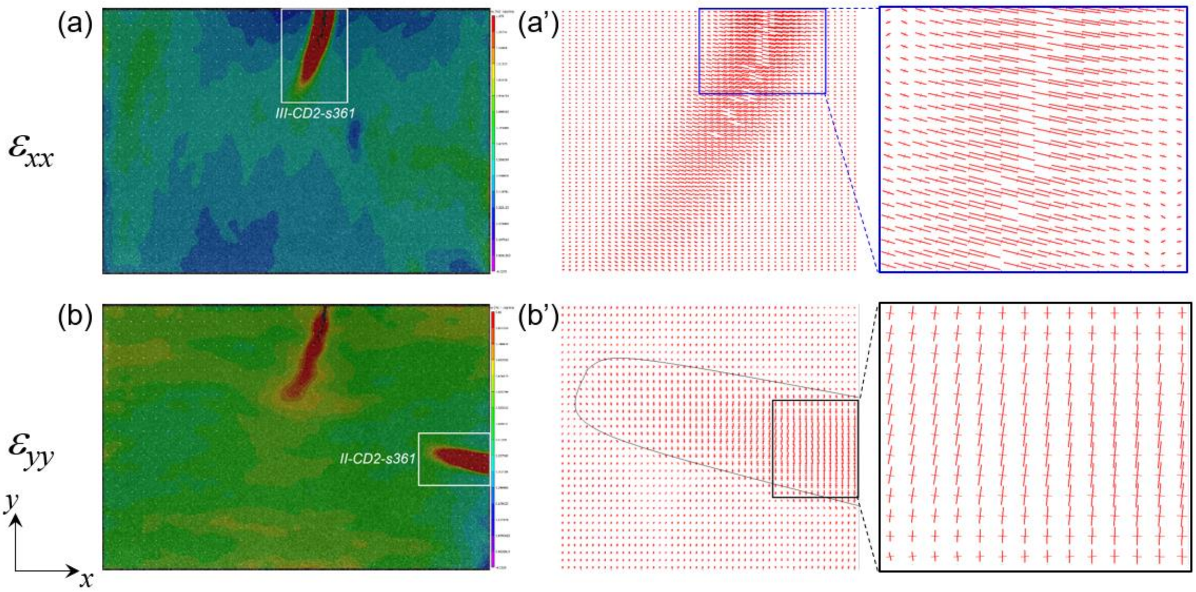

Figure 5. Identified cracks on ε_{xx} and ε_{yy} DIC maps and principal “mechanical” strains method (t = 161 h and w = 2.65%)

4. CONCLUSIONS

In this research, an experimental device based on both salt solutions technique and DIC method was developed in the laboratory. This allowed to perform controlled desiccation paths under different suction levels. Study is focused on characterizing shrinkage phenomenon and understanding cracks’ initiation.

According to this analysis, there is an influence of suction level on drying and shrinkage kinetics evolution: more suction increases, more the kinetic is faster. Furthermore, a shrinkage part of strains can be distinguished and completed by an additional part assumed as “mechanical”, acting cracks.

Cracking mechanism in mode I was observed under high suction level. Calculations of principal “mechanical” strains, without the shrinkage part, allowed confirming this mode of cracking. Thus, it can be assumed that cracks initiate when the “mechanical” strain part exceeds a critical value.

REFERENCES

Delage P., Howat M. D., Cui Y. J. 1998. The relationship between suction and swelling properties in a heavily compacted unsaturated clay. *Eng. Geology J*, 50, 31-48.

Fredlund D. G. and Rahardjo H. 1993. *Soil mechanics for unsaturated soils*. John Willey J.

Hammad T., Fleureau J. M. & Hattab M. 2013. Kaolin/montmorillonite mixtures behaviour on oedometric path and microstructural variations. *Eur. J. Env. Civ. Eng* 17, No. 9, 826–840.

Hattab M., Hammad T. & Fleureau J. M. 2014. Internal friction angle variation in a kaolin/montmorillonite clay mix and microstructural identification. *Géotechnique*, 65(1), 1–11.

Ighil Ameur L., Hattab M. 2022. Cracking of unsaturated clays using a newly developed small-beam bending apparatus and analysis by digital image correlation. *Geomechanics for Energy and the Environment*, 32, 100307. 10.1016/j.gete.2021.100307

Kodikara J. K., Barbour S. L., Fredlund D. G. 1999. Changes in clay structure and behavior due to wetting and drying. *Proc of the 8th Aust-NZ Conf on Geomech*, 179- 186.
Morris P. H., Graham J., Williams D. J. 1992. Cracking in drying soils. *Can. Geo. J*. 29, 263-277.
Wei X., Hattab M., Bompard P., Fleureau J. M. 2016. Highlighting some mechanisms of crack formation and propagation in clays on drying path. *Geotech. J*. 66(4), 287-300.
Wei X. 2014. Etude micro-macro de la fissuration des argiles soumises à la dessiccation. Doctoral dissertation, France.